# Enhancement of Contrast and Resolution of B-Mode Plane Wave Imaging (PWI) with Non-Linear Filtered Delay Multiply and Sum (FDMAS) Beamforming

Asraf Mohamed Moubark, Zainab Alomari, Sevan Harput, David M. J Cowell and Steven Freear
Ultrasound Group, School of Electronic and Electrical Engineering, University of Leeds, UK.
E-mail: elamm@leeds.ac.uk and S.Freear@leeds.ac.uk

***Abstract*—FDMAS has been successfully used in microwave imaging for breast cancer detection. FDMAS gained its popularity due to its capability to produce results faster than any other adaptive beamforming technique such as minimum variance (MV) which requires higher computational complexity. The average computational time for single point spread function (PSF) at 40 mm depth for FDMAS is 87 times faster than MV. The new beamforming technique has been tested on PSF and cyst phantoms experimentally with the ultrasound array research platform version 2 (UARP II) using a 3-8 MHz 128 element clinical transducer. FDMAS is able to improve both imaging contrast and spatial resolution as compared to DAS. The wire phantom main lobes lateral resolution improved in FDMAS by 40.4% with square pulse excitation signal when compared to DAS. Meanwhile the contrast ratio (CR) obtained for an anechoic cyst located at 15 mm depth for PWI with DAS and FDMAS are -6.2 dB and -14.9 dB respectively. The ability to reduce noise from off axis with auto-correlation operation in FDMAS pave the way to display the B-mode image with high dynamic range. However, the contrast to noise ratio (CNR) measured at same cyst location for FDMAS give less reading compared to DAS. Nevertheless, this drawback can be compensated by applying compound plane wave imaging (CPWI) technique on FDMAS. In overall the new FDMAS beamforming technique outperforms DAS in laboratory experiments by narrowing its main lobes and increases the image contrast without sacrificing its frame rates.**

## I. Introduction

Beamforming is a process of generating time delay that will be applied to a set of array at each time during transmission and reception. This is to focus and steer the beam pattern at intended region of interest (ROI). The most commonly used beamforming technique in medical ultrasound imaging is DAS technique. However, the final B-Mode image produced with DAS technique highly influenced by off-axis noise. To reduce the noise, apodization technique have been applied at transmitting and receiving stages. Even though this technique able to reduce the noise and side lobes but as trade off it increase the main lobes size which directly reduce the image resolution. Thus to overcome this issue, several new types of adaptive beamforming methods such as minimum variance and eigenvector minimum variance has been introduced [1]. These new beam formers able to dynamically change the receive aperture weights based on the received signals and able to increase the resolution and reduce side lobes but at expenses of high computational complexity and time. In order to improve the image resolution and contrast without increasing much the computational time, a new types of beamforming known as FDMAS which originally conceived in RADAR microwave system for breast cancer detection has been applied to PWI and CPWI [2]. Initial works on FDMAS carried out by [3] on linear array imaging with 2-cycle sinusoidal burst shows promising results. In this paper, we have explore the potential of this new non-linear beamforming technique with PWI and CPWI.

## II. Filtered Delay Multiply and Sum Beamforming

Initial process in FDMAS is same as DAS where each RF signal received at $i^{th}$ element, $S_i(t)$ will be aligned according to a set of calculated delay according to following equation:

$$\tau_i(x,z) = \frac{z\cos\theta + x\sin\theta + \frac{W}{2}\sin\theta}{c} + \frac{\sqrt{z^2 + (x_i - x)^2}}{c} \quad (1)$$

Where $\tau_i(x,z)$ is time required for the signal to reach field point located at axial and lateral location $x$ and $z$ respectively and return to $i_{th}$ element on the transducer, $W$ is physical width of the transducer, $c$ is speed of sound on the medium and finally $x_i$ is distance between $i_{th}$ element and centre of the transducer, $W/2$, and  is steering angle between transmitted signal and face of the transducer for each plane wave. Notice that $\theta$ will be zero for PWI. Instead of calculating time delay for each field point separately which will cause high computational time, a set of time delay vector can be computed in lateral direction, $z_{kl}$ where $k$ represent starting point of imaging and $l$ is the end point or depth of the image. The computed time delay vector added to the received RF signal, $S_i(t)$ is known as aligned RF signal, $V_i$ can be represented by following equation:

$$V_i = S_i(t - \tau_i(x, z_{kl})) \quad (2)$$

$$i = 1, 2, ..., 128$$

To form single B-Mode image line, a set of $N$ number $V_i$ needed. However, the summation process will not take place after the aligned process as in DAS beamforming technique but each frame or a set of aligned will gone through process similar to auto-correlation to form each image line as given by equation (3)

$$R_{FDMAS} = \sum_{i}^{N-1} \sum_{m}^{N} \text{sgn}\{V_i(t)V_m(t)\} \times \sqrt{|V_i(t)V_m(t)|} \quad (3)$$

Multiplying two RF signal with same frequency will eventually produce harmonics and DC components. Thus a bandpass filter applied on $R_{FDMAS}$ to extract its second harmonics. More details on mathematical operation explanation on FDMAS can be found on [3].

## III. Experiments

In order to study the effectiveness of FDMAS beamforming technique on PWI and CPWI, several laboratory experiments have been carried out on wire and multipurpose phantom with UARP II [4] [5]. Our first experiment was carried out on $120\mu m$ wire phantom located from 20 mm until 60 mm depth with 10 mm spacing between them as shown in Fig. 1. Our second experiment have been conducted on computerized imaging reference system (CIRS) multipurpose, multi tissue ultrasound phantom on hypoechoic cyst phantom.

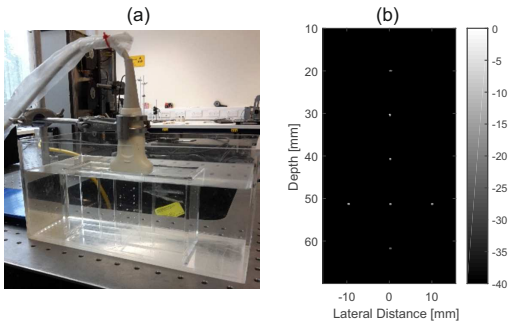


Fig. 1. (a) Wire phantom scanned with clinical transducer inside degas water and (b) its B-Mode model.

A broad band square pulse with 50 $ns$ duration have been employed on both experiments. A single B-Mode image was formed by compounding 1, 3, 5 and 7 PWI steered from $-15°$ to $+15°$ degree with increment of $5°$. The details for both experiments parameters are given in Table 1.

## IV. Performance Evaluation

In order to evaluate the final B-Mode images qualities formed with DAS and FDMAS beamforming techniques, several key performance indicator haven used. The main lobes resolution of PSF was measured on wire phantom located at 40 mm depth with Full width half maximum (FWHM), -6 dB. While the image CR and CNR of hypoechoic cyst was computed on CIRS phantom located at 15 mm depth. The

TABLE I
Experiments Parameters

| Properties | Wire Phantom | CIRS |
|---|---|---|
| Speed of Sound, m/s | 1480 | 1520 |
| Medium Attenuation, dB/MHz/cm | 0.22 | 0.5 |
| Transducer centre frequency, MHz | 5 | |
| Sampling Frequency, Tx/Rx, MHz | 160/80 | |
| No of Elements | 128 | |
| Bandwidth, % | 57 | |
| Excitation signals | Square Pulse | |
| Steering Angles | -15,-10,-5,0,+5,+10,+15 | |

CR is used to express the detectability of the object contrast between ROI inside the cyst and its background. While CNR is used the measure the cyst contrast with speckle or noise variation inside and outside of the cyst [6]. High CNR value means cyst can be visualize easily and the acoustic noise standard deviation is small or more uniform. Both CR and CNR equation are given by [6]

$$\text{CR(dB)} = 20\log_{10}(\frac{\mu_{cyst}}{\mu_{back}}) \quad (4)$$

$$\text{CNR(dB)} = 20\log_{10}(\frac{|\mu_{cyst} - \mu_{Back}|}{\sqrt{({\sigma_{cyst}}^2 + {\sigma_{Back}}^2)}}) \quad (5)$$

Where $\mu_{cyst}$ and $\mu_{Back}$ are means of image intensities inside and outside of the cyst respectively while ${\sigma_{cyst}}^2$ and ${\sigma_{Back}}^2$ are their variances. CR and CNR were calculated on the cysts by creating two different regions with the same dimensions. The first region is inside the cyst while the other region is located outside the cyst at the same depth. This is to ensure that the attenuation caused by frequency doesn't affect the measurements.

## V. Results and Discussion

The B-Mode images of PWI on wire phantom formed with DAS and FDMAS beamforming techniques using square pulse excitation signals is shown in Fig. 2 at 40 dB dynamic range.

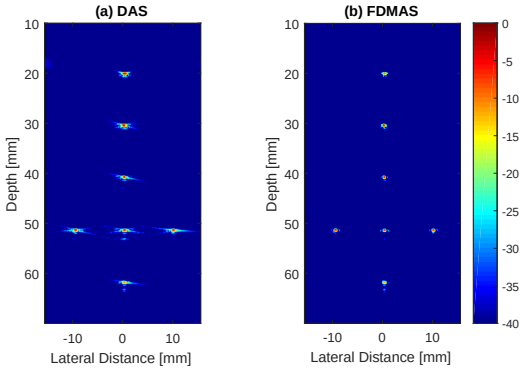


Fig. 2. Wire phantom B-Mode image for (a) DAS and (b) FDMAS.

It can be seen from Fig. 2(b) that the FDMAS significantly reduce more noises in lateral direction compared to axial direction. The lateral and axial normalized amplitude profiles presented in Fig. 3 for the wire phantoms also prove that the reduction of noises in lateral direction is more than in axial direction.

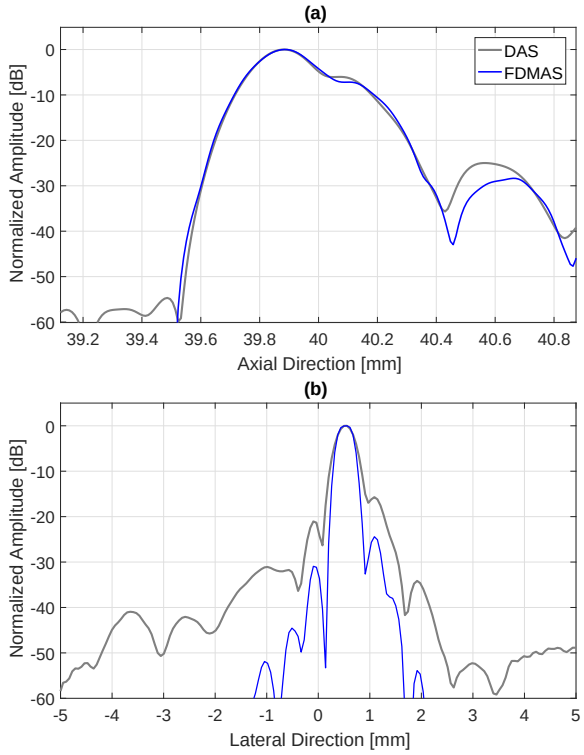


Fig. 3. Comparison of (a) axial and (b) lateral resolution of a wire phantom located at 40 mm depth with DAS and FDMAS beamforming techniques.

The spatial resolution at axial and lateral direction measured using function created by [7] at -6 dB main lobe width on wire phantom inside degas water at 40 mm depth. The results is presented in graphical form in Fig. 4. At $0^\circ$ steering angle, the lateral resolution measured at main lobes for DAS and FDMAS beamforming techniques employing pulse excitation signal are 0.49 mm and 0.41 mm respectively. The new non-linear beamforming technique shows 16.3% improvement when compared to traditional linear beamforming technique. The increment in the resolution getting better as the number of compounding increases from one to seven angles. The lateral resolution measured with CPWI of seven angles from $-15^\circ$ to $+15^\circ$ with increment of $5^\circ$ with DAS beamforming technique is 0.42 mm and 0.25 mm with FDMAS beamforming technique. This is 40.4% increment which is more than double compare to PWI.

The improvement on lateral resolution is expected since the auto-correlation process in FDMAS take place on that lateral direction and not in axial direction. The auto-correlation process produces maximum values when the same pattern signals detected and it reduces any unwanted side lobes or noises on the lateral direction. Meanwhile compounding

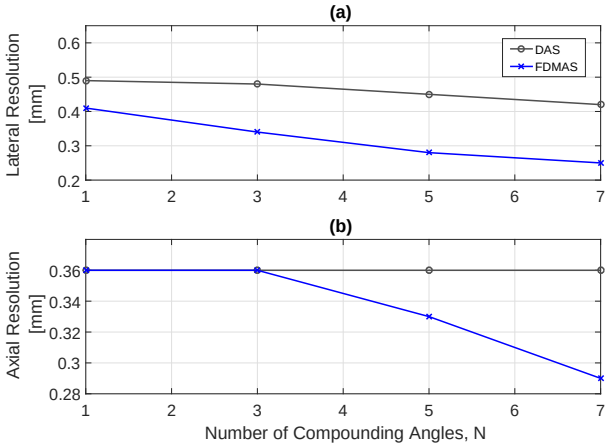


Fig. 4. (a) Lateral resolution and (b) axial resolution for wire phantom at 40 mm depth beam formed with DAS and FDMAS techniques and compounded with different number of angles.

process enhances the lateral resolution with FDMAS technique by averaging and cancelling the noises that present in lateral direction [8]–[10]. However, the same spatial improvement cant be seen on axial direction. As for axial direction, there is no significant change between DAS and FDMAS beamforming techniques with PWI and CPWI, N=3. The changes or minor improvement in axial resolution with FDMAS only starting to be visible at CPWI, N=5 and N=7. At N=5, the improvement in axial direction with FDMAS is 8.3% while with N=7 the improvement is 19.4%. Complete comparison on axial resolution between DAS and FDMAS is shown in Fig. 4.

The B-Mode images of PWI on 4.5 mm and 1.3 mm diameter CIRS hypoechoic cyst at 15 mm depth is shown in Fig. 5. The PWI considered as the worst case scenario produce very low quality B-mode images with DAS as shown in Fig. 5(a) yet FDMAS able to identify or map the location of 1.3 mm cyst as shown in Fig. 5 (b).

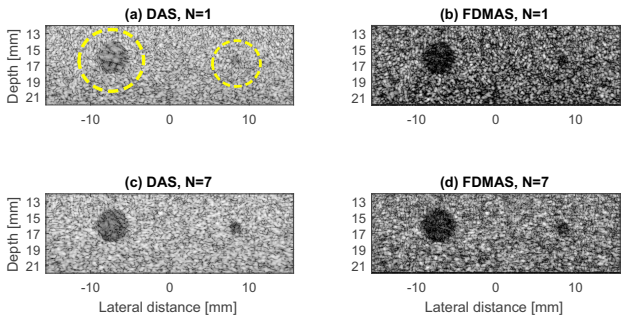


Fig. 5. B-Mode image of two hypoechoic cyst with (a) DAS, PWI, (b) FDMAS, PWI, (c) DAS, CPWI (N=7) and (d) FDMAS, CPWI (N=7) located at 15 mm depth with diameter of 4.5 mm and 1.3 mm displayed at 40 dB dynamic range.

The CR for PWI with DAS beamforming technique is -6.2 dB while with FDMAS is -14.9 dB. Increasing the compounding angles from one to seven eventually increase

the CR of the cystic region for DAS and FDMAS. With 7 compounding angles, the CR of DAS and FDMAS improves to -10.6 dB and -15.27 dB, respectively. However, the CR values difference between the two beamforming techniques decreases as the number of compounding angles increase from one to seven. In PWI, the CR improvement is 140.3% while with CPWI the improvement is only 44%. The reduction in CR gap between DAS and FDMAS can be related to the noise cancelation through increasing number compounding angles in DAS. Complete CR for both beamforming technique with different number of compounding angles is given in Fig. 6.

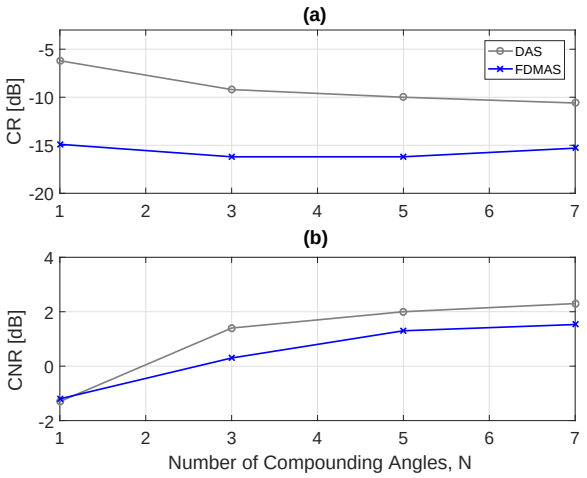


Fig. 6. (a) CR and (b) CNR for 4.5 mm diameter hypoechoic cyst located at 15 mm depth.

Another performance indicator used to evaluate FDMAS beamforming technique is CNR. The CNR values measured for PWI using square pulse as excitation signal is -1.3 dB and -1.2 dB for DAS and FDMAS respectively. AS the number of compounding angles increases into seven, the CNR values become 2.3 dB and 1.53 dB for DAS and FDMAS. The CNR values for FDMAS generally lower when compared to but it keep improving as number of compounding angels increasing. This is because, the auto-correlation process eliminate or reduce the small speckle or noise values that present outside the cyst. The area outside the cyst becomes non-uniform (high number of black and white spots) and causes high fluctuation between the speckle constructive and destructive region Thus it introduce extra black spots as can be seen on Fig. 5(b) and 5(d) compared to Fig. 5(a) and 5(c). On the other hand, DAS beamforming with CPWI reduce the speckle variation and produce more uniform region outside the cyst. As the compounding angles increases, the CNR values for DAS and FDMAS improves gradually. Complete CNR for both beamforming techniques with different number of compounding angles using square pulse excitation signal is given in Fig. 6.

## VI. Conclusion

A new type of non-liner beamforming technique known as FDMAS has been applied to PWI and CPWI using square pulse excitation signals. The performance parameters used to measure the B-Mode image performance shows that FDMAS produced better lateral resolution without any significant changes or small improvement on axial resolution. The image contrast also improve due to speckle noise reduction. Compounding technique significantly increase the spatial resolution on lateral direction and improve the image contrast. However, the CNR values are lower with FDMAS compared with DAS. This however can be overcome by CPWI and displaying the FDMAS at high dynamic range.

## References


[1] J.-F. Synnevag, A. Austeng, and S. Holm, "Benefits of minimum-variance beamforming in medical ultrasound imaging," *IEEE transactions on ultrasonics, ferroelectrics, and frequency control*, vol. 56, no. 9, pp. 1868–1879, 2009.

[2] H. B. Lim, N. T. T. Nhung, E.-P. Li, and N. D. Thang, "Confocal microwave imaging for breast cancer detection: Delay-multiply-and-sum image reconstruction algorithm," *IEEE Transactions on Biomedical Engineering*, vol. 55, no. 6, pp. 1697–1704, 2008.

[3] G. Matrone, A. S. Savoia, G. Caliano, and G. Magenes, "The delay multiply and sum beamforming algorithm in ultrasound b-mode medical imaging," *IEEE transactions on medical imaging*, vol. 34, no. 4, pp. 940–949, 2015.

[4] P. R. Smith, D. M. Cowell, B. Raiton, C. V. Ky, and S. Freear, "Ultrasound array transmitter architecture with high timing resolution using embedded phase-locked loops," *IEEE transactions on ultrasonics, ferroelectrics, and frequency control*, vol. 59, no. 1, pp. 40–49, 2012.

[5] C. A. Winckler, P. R. Smith, D. M. Cowell, O. Olagunju, and S. Freear, "The design of a high speed receiver system for an ultrasound array research platform," in *2012 IEEE International Ultrasonics Symposium*. IEEE, 2012, pp. 1481–1484.

[6] J. S. Ullom, M. Oelze, and J. R. Sanchez, "Ultrasound speckle reduction using coded excitation, frequency compounding, and postprocessing despeckling filters," in *2010 IEEE International Ultrasonics Symposium*. IEEE, 2010, pp. 2291–2294.

[7] S. Harput, J. McLaughlan, D. M. Cowell, and S. Freear, "New performance metrics for ultrasound pulse compression systems," in *2014 IEEE International Ultrasonics Symposium*. IEEE, 2014, pp. 440–443.

[8] Z. Alomari, S. Harput, S. Hyder, and S. Freear, "The effect of the transducer parameters on spatial resolution in plane-wave imaging," in *Ultrasonics Symposium (IUS), 2015 IEEE International*. IEEE, 2015, pp. 1–4.

[9] A. M. Moubark, Z. Alomari, S. Harput, and S. Freear, "Comparison of spatial and temporal averaging on ultrafast imaging in presence of quantization errors," in *Ultrasonics Symposium (IUS), 2015 IEEE International*. IEEE, 2015, pp. 1–4.

[10] Z. Alomari, S. Harput, S. Hyder, and S. Freear, "Selecting the number and values of the cpwi steering angles and the effect of that on imaging quality," in *2014 IEEE International Ultrasonics Symposium*. IEEE, 2014, pp. 1191–1194.